Supporting Figure S1

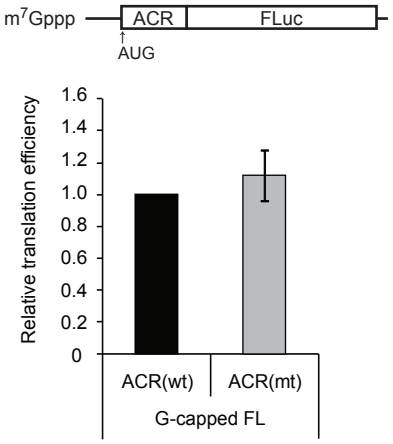

Supporting Figure S2

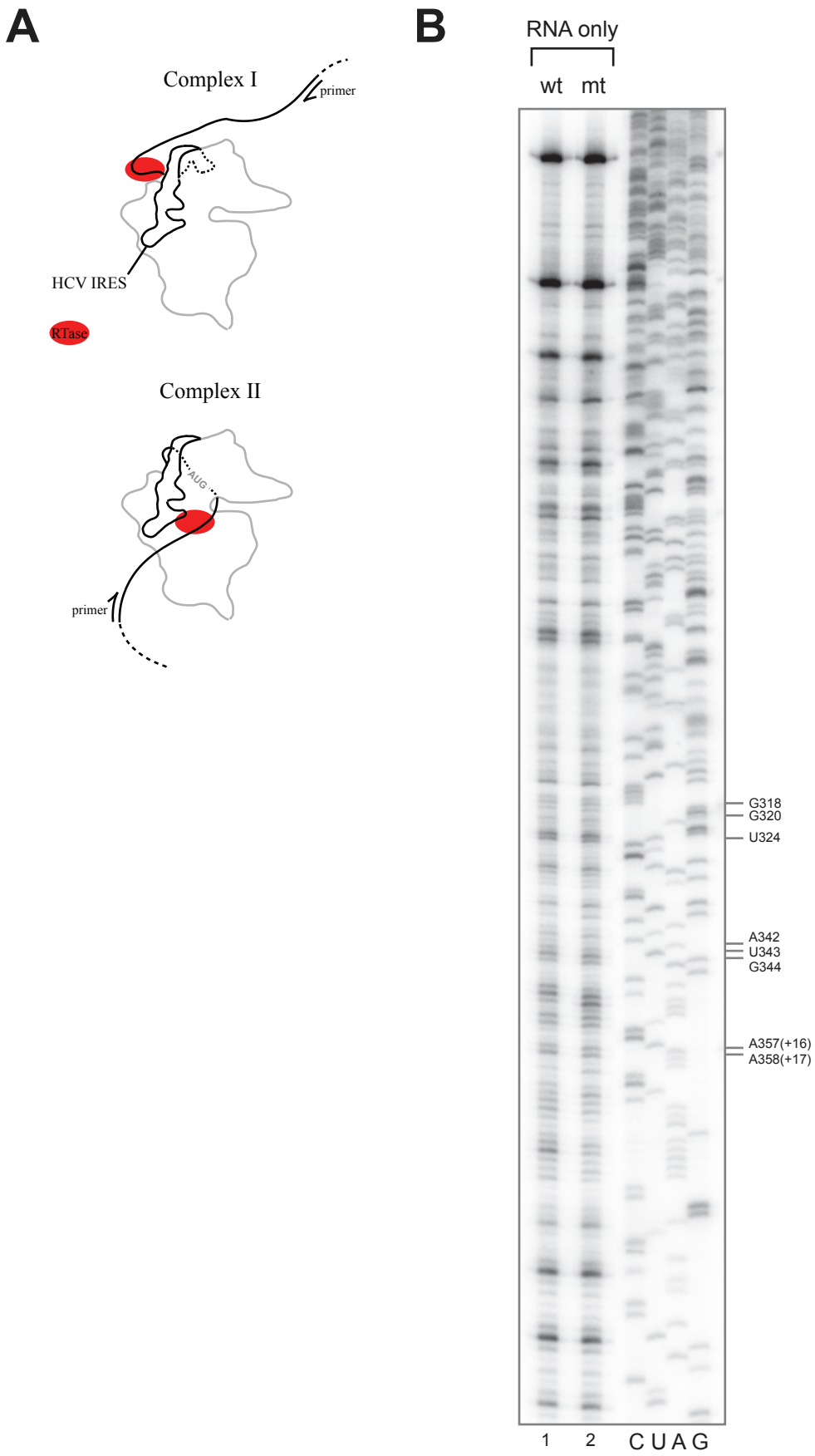

Supporting Figure S3

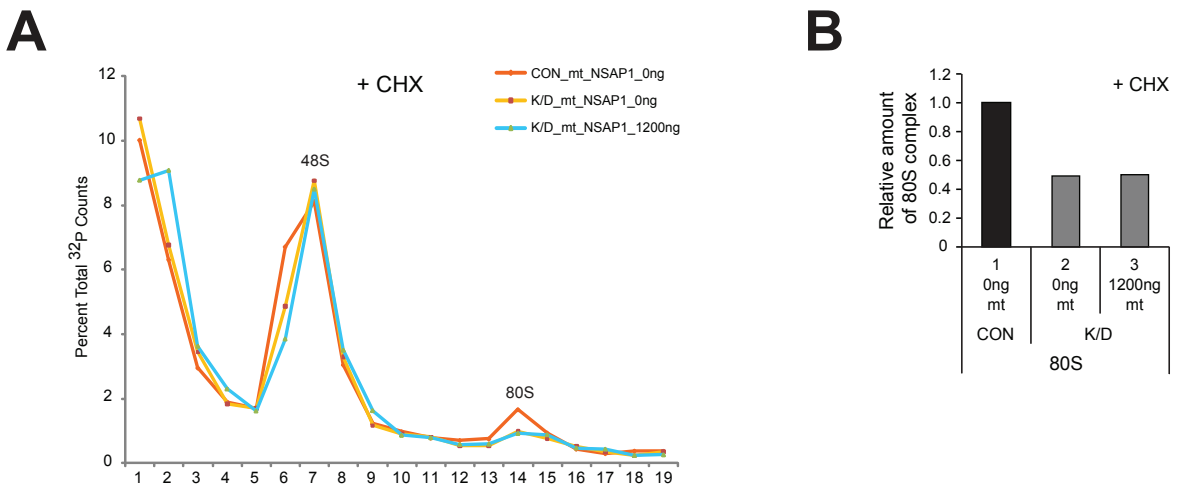

Supporting Figure S4

A

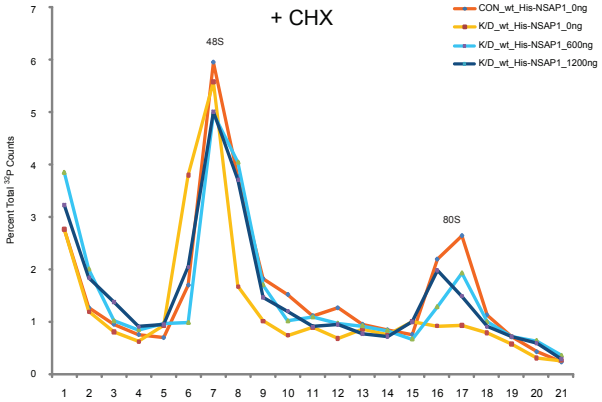

B

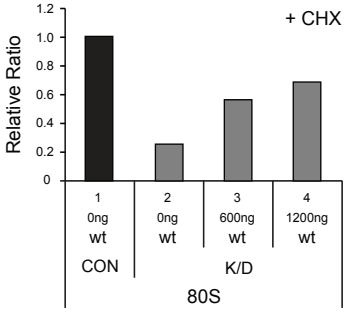

Supporting Figure S5

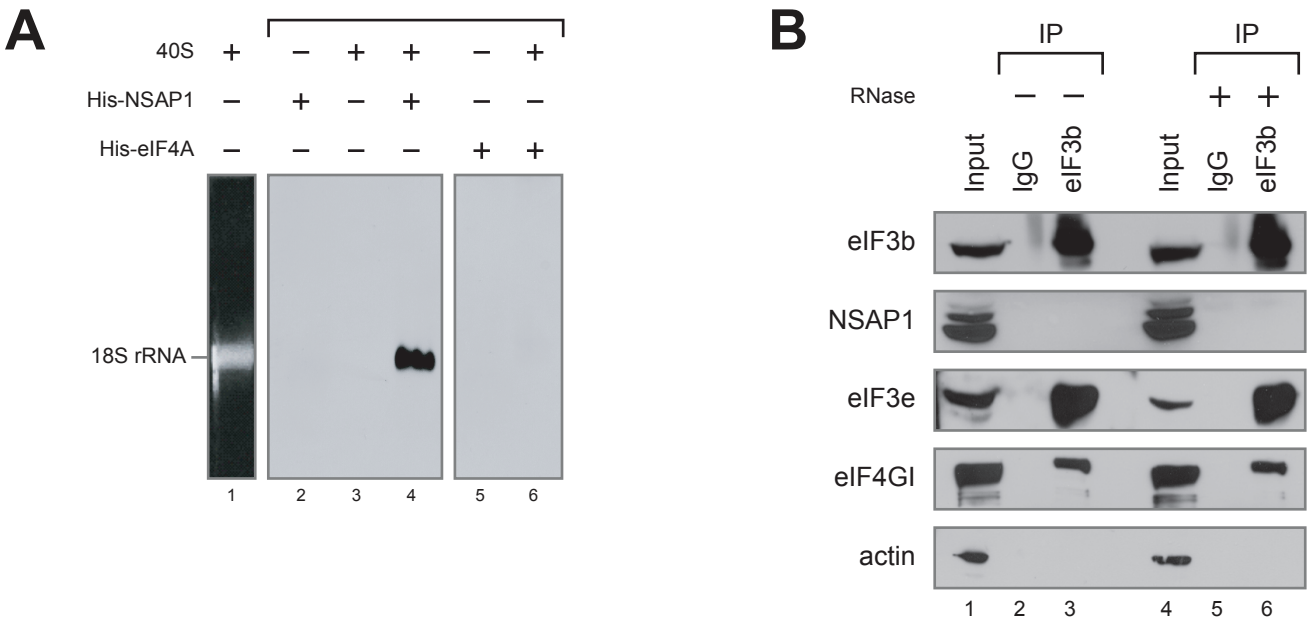

Supporting figure legends

Figure S1. A to G substitution in ACR does not affect translation at the elongation step. In order to test whether the A to G substitutions in the ACR mutant affect translation at the elongation step, we generated cap-dependent reporter mRNAs containing either wild-type ACR or mutant ACR downstream of the initiation codon. The reporter gene (firefly luciferase) is fused in frame with the oligopeptides encoded by the ACR. The mRNAs contain the same 5'UTR of 22 nucleotides which directs translation of the reporter in the scanning mode. In vitro transcription was performed to produce 5' capped mRNAs using template DNA pACRF_wt (wild-type) or pACRF_mt (mutant). These DNAs were constructed by self-ligation of the Asp718-AccI-Klenow-treated DNA fragment from pH374F_wt and pH374F_mt, respectively. In vitro translation was performed in RRL, and the relative translation efficiency is depicted (lower panel). Translational efficiency of the capped wild-type ACR mRNA was the same as that of the capped mutant ACR mRNA. This indicates that the translation reduction shown in Figure 1B is not due to the reduction in translation elongation rate caused by the mutation.

Figure S2. Toeprint analyses of wild-type and mutant HCV mRNAs. (A) Schematic diagram of toeprinting process depicting how the bands of complexes I and II are generated by the pausing of reverse transcriptase at different sites of the HCV RNA bound to 40S ribosomal subunit. The reverse transcriptase is symbolized by an oval. (B) No change in toeprints at the +16 and +17 positions due to the ACR A to G mutations was observed when RRL was not included in the reaction mixture with the RNAs. The

toeprint data were obtained by phosphorimaging after resolving primer-extended samples on a 6% sequencing gel.

Figure S3. The effect of NSAP1 on 80S complex formation on the mutant HCV mRNA. (A) The effect of NSAP1 on 80S complex formation was monitored by sucrose gradient analyses of NSAP1-depleted and NSAP1-replete lysates. The labeled mutant HCV RNAs were incubated in control (CON) or NSAP1-depleted lysates (K/D) in the presence of cycloheximide (CHX), and then subjected to sucrose gradient analyses. The effect of NSAP1 supplementation on 80S complex formation was observed by adding purified Flag-NSAP1 protein (1200 ng) to NSAP1-depleted lysates. The radioactivity (^{32}P-labeled mutant IRES [18-374 nt]) in each fraction of the 5%–20% sucrose gradient is depicted as a percentile in the graph. (B) Relative amount of 80S complex on the mutant HCV IRES quantified from panel A.

Figure S4. NSAP1 purified from *E. coli* restores 80S complex formation on the HCV IRES. (A) The effect of His-NSAP1 from *E. coli* on 80S complex formation was monitored by sucrose gradient analyses as described in Fig. 3C. (B) Relative amount of 80S complex on the wild type HCV IRES quantified from panel A.

Figure S5. NSAP1 specifically interacts with 40S ribosome, but not with translation factors tested. (A) Co-migration of purified 40S ribosomal subunits and His-NSAP1 on a 1% agarose gel was observed by ethidium bromide staining (lane 1) or Western blotting with an antibody against the His tag (lanes 2–6). (B) Immunoprecipitation experiments

were performed with 293T cell extracts using an antibody against eIF3b or a control antibody against normal goat IgG. Co-immunoprecipitated proteins were visualized by Western blotting with antibodies against eIF3b, NSAP1, eIF3e, eIF4G, and actin. (C) Purified 40S ribosomal subunits were not contaminated with other proteins. Western blot analyses of purified 40S ribosomal subunits were performed using antibodies against RpS6, NSAP1, eIF3b, eIF4GI, eIF4AI, eIF2α, PABP and eIF4E.